



## Flexural strength prediction for cold-formed steel sections unsymmetric about the axis of bending

Robert S. Glauz<sup>1</sup>, Benjamin W. Schafer<sup>2</sup>

### Abstract

The Direct Strength Method (DSM) is useful in determining the local and distortional buckling strength of thin-walled cold-formed steel compression and flexural members. This method provides a consistent approach applicable to any cross-section based on its yielding and elastic buckling characteristics. Recent research has shown opportunity for improvement for flexural members unsymmetric about the axis of bending. This paper investigates how additional stress redistribution due to asymmetry impacts strength. Adjustments to the DSM strength equations for local and distortional buckling are proposed to account for this behavior, and are validated against a wide variety of test and simulation results. A new form of the DSM strength equations is also developed to additionally address cases where section instability results in a reduced effective depth and therefore lower strength. This new proposed form offers simplicity and broader applicability suitable for consideration in design specifications.

### 1. Introduction

The strength of cold-formed steel members subject to local and distortional buckling can be determined using the Direct Strength Method (DSM) as provided in the AISI S100 (AISI 2016) and AS/NZS 4600 (AS/NZS 2018) specifications. This DSM strength is a function of the yielding and elastic buckling behavior of the section, enabling a consistent approach regardless of section complexity.

For flexural members, DSM uses the dimensionless slenderness factors  $\lambda_L = \sqrt{M_y/M_{crL}}$  and  $\lambda_D = \sqrt{M_y/M_{crD}}$  where  $M_y$  is the moment causing first yield, and  $M_{crL}$  and  $M_{crD}$  are the critical elastic buckling moments for local and distortional buckling, respectively. The strength equations utilize a form of the Winter plate buckling formula:

$$\frac{M_{nL}}{M_y} = (1 - 0.15/\lambda_L^{0.8})/\lambda_L^{0.8} = \left[ 1 - 0.15 \left( \frac{M_{crL}}{M_y} \right)^{0.4} \right] \left( \frac{M_{crL}}{M_y} \right)^{0.4} \quad (1)$$

$$\frac{M_{nD}}{M_y} = (1 - 0.22/\lambda_D)/\lambda_D = \left[ 1 - 0.22 \left( \frac{M_{crD}}{M_y} \right)^{0.5} \right] \left( \frac{M_{crD}}{M_y} \right)^{0.5} \quad (2)$$

<sup>1</sup> Owner, RSG Software, Inc., Lee's Summit, MO 64081, glauz@rsgsoftware.com

<sup>2</sup> Professor, Johns Hopkins University, Baltimore, MD 21218, schafers@jhu.edu

where  $M_{nL}$  and  $M_{nD}$  are the nominal moment strengths for local and distortional buckling, respectively. These equations are used for strengths up to the yield moment as plotted in Fig. 1. The AISI (2016) provisions define the strength above the yield moment as a separate inelastic reserve linear transition to the plastic moment strength.

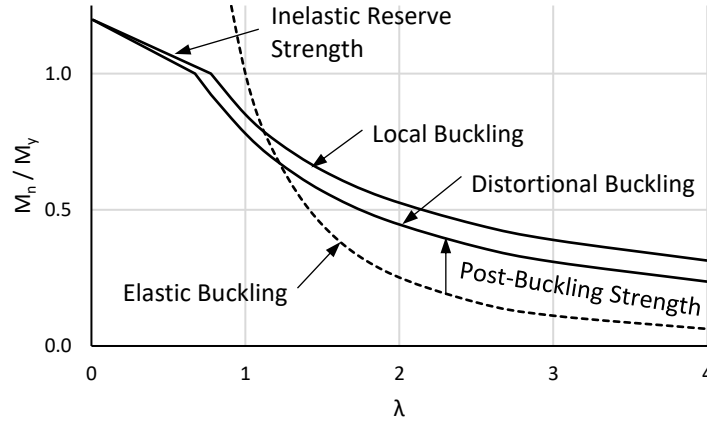


Figure 1. Current DSM strength curves in AISI S100-16.

DSM has been used successfully for several years, but some opportunities for continued improvement exist (Schafer 2019). In particular, tests and simulations of flexural members unsymmetric about the axis of bending often demonstrate under-prediction and sometimes over-prediction with DSM. Studies by Baur and LaBoube (2001), Nuttayasakul and Easterling (2003), Oey and Papangelis (2020), Degtyarev (2020), and Raebel and Gwozdz (2017) have investigated different DSM equations for special cases, as shown in Fig. 2.

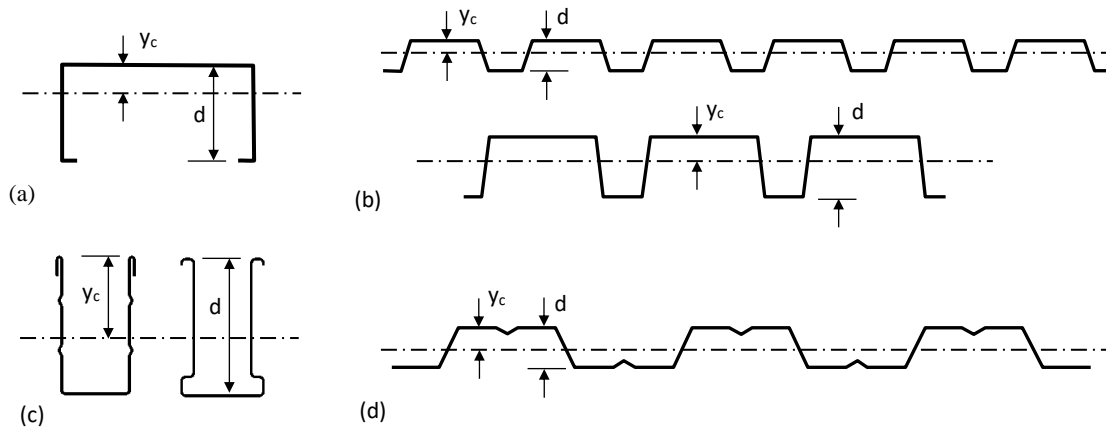


Figure 2. Examples of sections not symmetric about the axis of bending.

This paper presents a generalized modification to the DSM strength predictions for sections unsymmetric about the axis of bending while maintaining equivalent strength predictions for sections symmetric about the axis of bending. A new simpler form of the DSM strength equation is also presented which better accommodates certain types of sections that experience more strength reduction due to their inability to maintain full section depth.

## 2. Modification to DSM strength curves

The general form of the DSM strength equation is given by Eq. 3, where the exponent  $\eta$  and coefficient  $c$  provide flexibility to fit the equation to strengths observed in tests. The  $\lambda_1$  limit is the slenderness at which first yield occurs ( $M_n/M_y = 1$ ). For slenderness less than  $\lambda_1$ , The DSM strength for inelastic reserve is given by the linear expression shown in Eq. 4 between  $(0, k_s)$  and  $(\lambda_1, 1)$ , where  $k_s$  is the shape factor determined by the ratio of plastic section modulus to elastic section modulus, i.e.,  $k_s = M_p/M_y$  where  $M_p$  is the plastic moment.

$$\text{For } \lambda > \lambda_1: \frac{M_n}{M_y} = \frac{1}{\lambda^\eta} - \frac{c}{\lambda^{2\eta}} = (1 - c/\lambda^\eta)/\lambda^\eta \quad (3)$$

$$\text{For } \lambda \leq \lambda_1: \frac{M_n}{M_y} = 1 + (k_s - 1)(1 - \lambda/\lambda_1) \quad (4)$$

Sections unsymmetric about the axis of bending often undergo greater redistribution of stresses as the moment increases. Stress redistribution may be driven by material nonlinearity where yielding in the tension and compression regions are unbalanced as shown in Fig. 3(b), or by geometric nonlinearity where slender portions of the cross-section cannot carry their full elastic stress as shown in Fig. 3(c), or by a combination of these two as shown in Fig. 3(d). Both types of stress redistribution result in a shift of the neutral axis to maintain net-zero axial force, typically more than that for a section symmetric about the axis of bending.

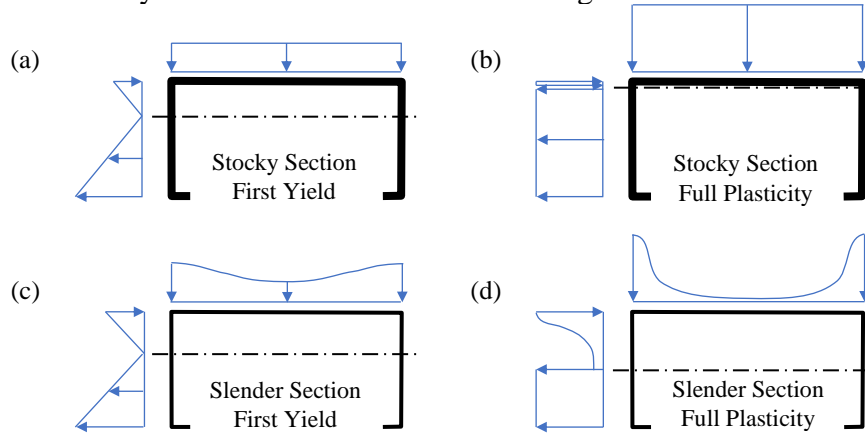


Figure 3. Stress redistribution due to (b) material nonlinearity, (c) geometric nonlinearity, and (d) both.

The exponent  $\eta$ , coefficient  $c$ , and slenderness limit  $\lambda_1$  require adjustment to reflect the difference in strength observed in tests for sections unsymmetric about the axis of bending. The magnitude of adjustment has correlated well with the relative position of the elastic neutral axis, which is defined by the expression in Eq. 5. This non-dimensional symmetry parameter  $\beta_s$  can be expressed using the extreme compression fiber distance ( $y_c$ ) and overall depth ( $d$ ), or the ratio of section moduli for compression ( $S_c$ ) and tension ( $S_t$ ). For a section symmetric about the axis of bending,  $\beta_s=1$ ; for a section with first yield in tension,  $\beta_s<1$  and the strength curve should be higher; and for a section with first yield in compression,  $\beta_s>1$  and the strength curve should be lower.

$$\beta_s = \frac{2y_c}{d} = \frac{2}{1+S_c/S_t} \quad (5)$$

This coefficient was found to work well as a direct multiplier on the exponents currently used for local (0.8) and distortional buckling (1.0). For local buckling, the exponent  $\eta_L$  becomes  $0.8\beta_s$  with possible values ranging from 0 to 1.6. For distortional buckling, the exponent  $\eta_D$  becomes  $1.0\beta_s$  with possible values ranging from 0 to 2. At one extreme, where  $\eta=0$ , the curve is a horizontal line at  $M_n/M_y=1$ . At the other extreme, where  $\eta=2$ , the curve is an offset from the elastic buckling curve.

The slenderness limit  $\lambda_1$  has been observed to increase (shift right) as the strength curve raises ( $\beta_s$  decreases), and also as the shape factor  $k_s$  increases. These adjustments were found to work well as direct divisors and multipliers, respectively:  $\lambda_1=\lambda_{10}(\beta_{so}/\beta_s)(k_s/k_{so})$ , where  $\lambda_{10}$  is the base slenderness limit currently used in DSM,  $\beta_{so}$  is the base symmetry factor (1.0), and  $k_{so}$  is the base shape factor.

Typical cold-formed steel sections such as those used to calibrate the DSM strength curves have a shape factor  $k_s$  near 1.2. Evaluation of the SFIA (2018) studs and tracks shows similar shape factors for major axis bending around 1.2 as shown in Table 1. Therefore, a base shape factor of 1.2 was chosen in the slenderness limit adjustment. The range of shape factors and symmetry factors for minor axis bending of SFIA studs and tracks are also given in Table 1.

Table 1. Shape factor data for SFIA (2018) studs (without holes) and tracks

Type	Bending		$k_s = M_p/M_y$	$\beta_s = 2y_c/d$
	About	Sections	Mean (CoV)	Range
Stud	Major Axis	428	1.19 (0.04)	1.00
Track	Major Axis	283	1.23 (0.06)	1.00
Stud	Minor Axis <sup>c</sup>	428	1.51 (0.04)	0.30 – 0.78
Track	Minor Axis <sup>c</sup>	283	1.76 (0.03)	0.17 – 0.63
Stud	Minor Axis <sup>t</sup>	428	1.51 (0.04)	1.22 – 1.70
Track	Minor Axis <sup>t</sup>	283	1.76 (0.03)	1.37 – 1.83

<sup>c</sup> Web in compression, <sup>t</sup> Web in tension

The adjustments described herein are incorporated into the DSM equations as follows, where the coefficients  $c_L$  and  $c_D$  are determined by satisfying the strength equations for  $M_n/M_y=1$  at  $\lambda=\lambda_1$ .

$$\text{For } \lambda_L \leq \lambda_{1L}: M_{nL} = M_y + (M_p - M_y)(1 - \lambda_L/\lambda_{1L}) \quad (6)$$

$$\text{For } \lambda_L > \lambda_{1L}: M_{nL} = \left[ 1 - c_L \left( \frac{M_{crL}}{M_y} \right)^{0.4\beta_s} \right] \left( \frac{M_{crL}}{M_y} \right)^{0.4\beta_s} M_y \quad (7)$$

$$\lambda_{1L} = 0.776 \left( \frac{k_s}{1.2\beta_s} \right) \quad (8)$$

$$c_L = \left( 1 - \lambda_{1L}^{0.8\beta_s} \right) \lambda_{1L}^{0.8\beta_s} \quad (9)$$

$$\text{For } \lambda_D \leq \lambda_{1D}: M_{nD} = M_y + (M_p - M_y)(1 - \lambda_D/\lambda_{1D}) \quad (10)$$

$$\text{For } \lambda_D > \lambda_{1D}: M_{nD} = \left[ 1 - c_D \left( \frac{M_{crD}}{M_y} \right)^{0.5\beta_s} \right] \left( \frac{M_{crD}}{M_y} \right)^{0.5\beta_s} M_y \quad (11)$$

$$\lambda_{1D} = 0.673 \left( \frac{k_s}{1.2\beta_s} \right) \quad (12)$$

$$c_D = \left( 1 - \lambda_{1D}^{\beta_s} \right) \lambda_{1D}^{\beta_s} \quad (13)$$

### 3. Proposed new form of strength curves

The wide range of the strength curve exponents used in Eqs. 7 and 11 is a departure from the philosophy that a buckling mode is associated with a specific power curve ( $\lambda^2$  for elastic buckling,  $\lambda^{0.8}$  for local buckling,  $\lambda^{1.0}$  for distortional buckling), rendering it as merely one of many mathematical forms capable of being calibrated to test data. Although this form is a descendent of the Winter plate buckling formula and provides flexibility to handle many cases, additional empirical adjustments are necessary for certain cases. It also exhibits a discontinuity at yield not observed in tests.

A broader variety of cases could be accommodated more naturally with a different slenderness-based equation form where modifiers are driven more directly by the influences of shape factor, stress redistribution, and residual strength at high slenderness. One such novel form of the strength curve was developed to capture strength prediction throughout the entire range of slenderness values including inelastic reserve. The general form of this equation is:

$$\frac{M_n}{M_p} = \frac{1+a\lambda^2}{1+b\lambda^2} = \frac{M_{cr}+aM_y}{M_{cr}+bM_y} \quad (14)$$

This form of the strength curve exhibits several notable features:

- At zero slenderness, the magnitude is 1 and the slope with respect to  $\lambda$  is zero.
- The horizontal asymptote is  $a/b$ , and for  $a/b < 1$  the slope of the curve is always negative.
- The steepest slope (inflection point) occurs at  $\lambda=1/\sqrt{3b}$ .
- For a given  $a/b$  ratio, smaller values of  $a$  and  $b$  produce a more gradual approach to the asymptote, thus providing a means to calibrate the curvature.
- For  $a \geq 0$  and  $b < k_s$ , the strength curve always crosses the elastic buckling curve, the point at which post-buckling strength begins.
- For  $a = 0$  and  $b \geq k_s$ , the curve stays below the elastic buckling curve.

For local buckling, the base coefficients  $a$  and  $b$  were determined by matching the curve to the current DSM provisions for both inelastic reserve strength and local buckling strength (Eq. 1) as shown in Fig. 4(a) and given in Eq. 15.

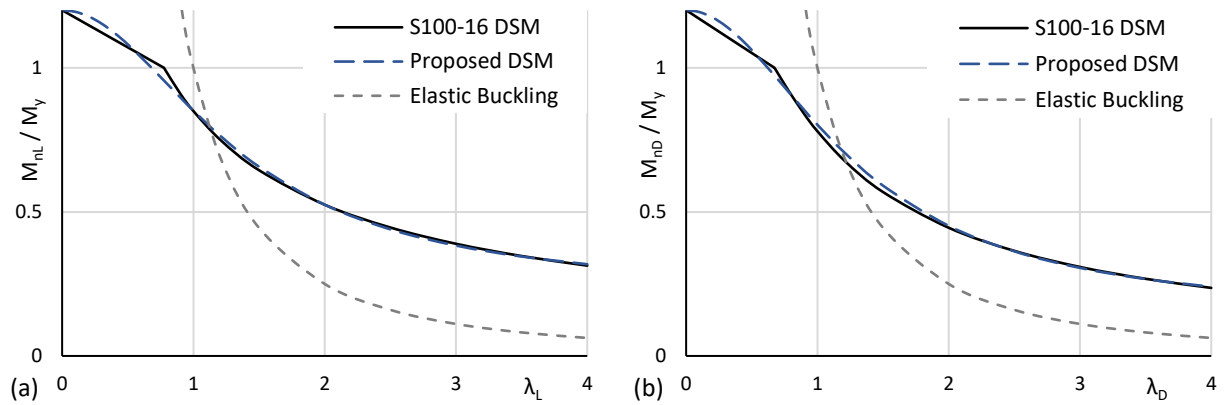


Figure 4. Curve comparison for (a) local buckling and (b) distortional buckling

$$M_{nL} = k_s M_y \frac{1+0.10\lambda_L^2}{1+0.55\lambda_L^2} = M_p \frac{M_{crL}+0.10M_y}{M_{crL}+0.55M_y} \quad (15)$$

The shape factor  $k_s$  is already incorporated into Eq. 15, but adjustments are required for members unsymmetric about the axis of bending, where stress redistribution and degradation of residual strength can have additional influence. These adjustments were implemented using coefficients  $\alpha_s$  and  $\beta_s$  as follows:

$$M_{nL} = M_p \frac{M_{crL} + 0.10\alpha_s M_y}{M_{crL} + 0.55\beta_s M_y} \quad (16)$$

$$\alpha_s = d_s/d \quad \beta_s = 2y_c/d$$

The  $\alpha_s$  coefficient addresses the potential reduction in strength at higher slenderness for sections unable to maintain full section depth, where  $d_s$  is the depth of the stable portion of the section remaining after local buckling at extreme slenderness, typically full depth ( $d$ ) or no depth (0).

The  $\beta_s$  coefficient is the same symmetry factor used as a modifier to the DSM curves to account for stress redistribution associated with asymmetry. It is applied in the denominator to alter coefficient  $b$  which has more influence over the entire curve. This simple multiplier provided good results using this equation form. For a section with first yield in tension,  $\beta_s < 1$ , and the strength curve is higher. For a section with first yield in compression,  $\beta_s > 1$ , and the strength curve is lower.

For distortional buckling, the base coefficients  $a$  and  $b$  were determined by matching the curve to the current DSM provisions for both inelastic reserve strength and distortional buckling strength (Eq. 2) as shown in Fig. 4(b) and given in Eq. 17.

$$M_{nD} = k_s M_y \frac{1 + 0.07\lambda_D^2}{1 + 0.60\lambda_D^2} = M_p \frac{M_{crD} + 0.07M_y}{M_{crD} + 0.60M_y} \quad (17)$$

The same  $\alpha_s$  and  $\beta_s$  coefficients are applied to distortional buckling to account for stress redistribution and residual strength reduction at high slenderness for sections unsymmetric about the axis of bending.

$$M_{nD} = M_p \frac{M_{crD} + 0.07\alpha_s M_y}{M_{crD} + 0.60\beta_s M_y} \quad (18)$$

$$\alpha_s = d_s/d \quad \beta_s = 2y_c/d$$

#### 4. Validation of modified and proposed DSM curves

The current AISI DSM equations were established by calibrating the coefficients and exponents to a large number of tests and wide variety of sections which were originally categorized as prequalified sections (Schafer and Peköz 1998, Yu and Schafer 2003, 2006, 2007). The LRFD resistance factor of 0.9 for flexural members was justified based on the DSM accuracy for those sections with a target reliability index of 2.5. The following validations involve other types of sections and more recent studies which require the modifications to the strength predictions presented herein to achieve similar or better reliability.

##### 4.1 Sections unsymmetric about axis of bending

Oey and Papangelis (2020) performed a computational study of stiffened C sections in minor-axis bending with the web in compression. Nonlinear finite element simulations were run on 33 sections having slenderness  $\lambda_L$  between 0.633 and 4.0,  $k_s$  between 1.43 and 1.66, and  $\beta_s$  between 0.50 and 0.66. The full section depth is stable for these local buckling cases ( $\alpha_s=1$ ).

Simulations for a variety of deck sections were performed by Degtyarev (2020), consisting of many common stiffened and unstiffened profiles with designations of 1F, 1.5B, 1.5BR, 3N, and 3NR. The unstiffened profiles were controlled by local buckling and the stiffened profiles were controlled primarily by distortional buckling. Some profiles had equal top and bottom flanges where  $\beta_s = 1$ , whereas others had  $\beta_s$  values ranging from 0.74 to 1.26.

A series of plain channel sections in minor axis bending were tested by Beale, Godley, and Enjily (2001). The tests were performed with the free edges in compression and were controlled by local buckling. The tested sections varied in slenderness, but had similar proportions with  $k_s$  between 1.78 and 1.86, and  $\beta_s$  between 1.48 and 1.50. Predictions for these tests used a stable depth factor of  $\alpha_s=0$  which lowers the strength at higher slenderness. Two of the tests at low slenderness had strengths well above  $M_p$  and were therefore excluded from this evaluation.

A number of complex hat sections, typically used as truss chords, were tested by Baur and LaBoube (2001) and Nuttayasakul and Easterling (2003). The tests were performed with the edges of the stiffened flanges in compression and were controlled by distortional buckling. Although these tests consisted of a variety of different shapes, their strength modification characteristics were similar. The shape factor  $k_s$  varied from 1.27 to 1.48, and  $\beta_s$  varied from 0.99 to 1.19. Predictions for these tests used a stable depth factor of  $\alpha_s=0$  which lowers the strength at higher slenderness.

The statistics for the DSM prediction methods are tabulated in Table 2. For local buckling, the modified and proposed new DSM predictions show significant improvement over the current DSM. For distortional buckling, the modified DSM provides minor improvement and the proposed new DSM shows marked improvement particularly for the complex hat shapes.

Table 2. Comparison of tests and simulations to predictions ( $M_t/M_n$ )

Researchers	Shape <sup>a</sup>	Mode <sup>b</sup>	Type <sup>c</sup>	Tests <sup>d</sup>	S100-16 DSM Mean (CoV)	Modified DSM Mean (CoV)	Proposed DSM Mean (CoV)
Beale et al. (2001)	T	LB	Test	11	0.97 (0.19)	1.10 (0.10)	1.00 (0.15)
Baur and LaBoube (2001)	H	DB	Test	48	0.92 (0.32)	0.95 (0.31)	1.09 (0.24)
Nuttayasakul and Easterling (2003)	H	DB	Test	67	1.02 (0.26)	1.10 (0.24)	1.12 (0.18)
Combined				126	0.98 (0.30)	1.04 (0.26)	1.10 (0.21)
Oey and Papangelis (2020)	C	LB	Sim	33	1.98 (0.12)	1.08 (0.07)	1.05 (0.08)
Degtyarev (2020)	D	LB	Sim	156-172	1.22 (0.14)	1.12 (0.05)	1.11 (0.05)
Degtyarev (2020)	D	DB	Sim	153-168	1.05 (0.07)	1.03 (0.05)	1.05 (0.06)
Combined				342-373	1.21 (0.21)	1.08 (0.06)	1.08 (0.06)
All Combined				468-499	1.15 (0.23)	1.07 (0.14)	1.08 (0.12)

<sup>a</sup> C=Lipped Channel, D=Deck, H=Hat, T=Track

<sup>b</sup> LB=Local buckling, DB=Distortional buckling

<sup>c</sup> Sim=Simulations, Test=Physical Tests

<sup>d</sup> Number varied by method due to controlling limit state

#### 4.2 Legacy data

The original DSM development work by Schafer and Peköz (1998) evaluated a large database of 574 cold-formed steel tests from 17 different studies. This same test data was evaluated using the

modified and proposed new DSM as summarized in Table 3. This evaluation also included two later studies (Yu and Schafer 2003, 2006) consisting of 26 C sections and 20 Z sections. The data in Table 3 excludes hat section tests by one study due to uncertainty about the test methods and results, but retains all other hat section data from four other studies which showed much better agreement.

Table 3. Comparison of legacy tests to predictions ( $M_u/M_n$ )

Axis of Bending	Mode <sup>a</sup>	Tests	S100-16 DSM	Modified DSM	Proposed DSM
			Mean (CoV)	Mean (CoV)	Mean (CoV)
Symmetric	LB	147	1.01 (0.09)	1.02 (0.09)	1.03 (0.09)
Symmetric	DB	232	1.07 (0.12)	1.08 (0.12)	1.07 (0.12)
Unsymmetric	LB	69	1.15 (0.23)	1.07 (0.10)	1.06 (0.10)
Unsymmetric	DB	140	1.12 (0.13)	1.08 (0.13)	1.08 (0.13)
Combined		588	1.08 (0.14)	1.06 (0.11)	1.06 (0.11)

<sup>a</sup> LB=Local buckling, DB=Distortional buckling

The sections identified as symmetric about the axis of bending were C and Z sections, some trapezoidal deck sections, and a few hat sections with a mid-depth neutral axis. All three prediction methods are essentially equivalent for both local and distortional buckling because  $\beta_s \approx 1.0$  and  $k_s \approx 1.2$  for these tests. The sections identified as unsymmetric about the axis of bending were hat sections and some trapezoidal deck sections, where  $\beta_s$  ranged from 0.63 to 1.24 and  $k_s$  ranged from 1.07 to 1.36. The modified and proposed DSM predictions provided considerable improvements for local buckling and slight improvements for distortional buckling. Overall, the modified and proposed DSM predictions provided nearly identical improvement because all of these tested sections had full stable depth ( $\alpha_s=1$ ).

The results in Table 3 demonstrate that the initial objective of this study was achieved. The mean and CoV values for the symmetric cases are essentially unchanged, whereas the mean and CoV for the unsymmetric cases show significant improvement.

## 5. Conclusions

Modifications to the DSM equations for local and distortional buckling of flexural members were developed to capture the influence of shape factor and stress redistribution due to material and geometric nonlinearity for members unsymmetric about the axis of bending. These modifications were validated against a variety of tests and simulations, where significant improvement in accuracy were achieved for local buckling, and minor improvements were seen for distortional buckling. For complex hat shapes subject to distortional buckling, additional modifications to the standard form of the DSM equation are needed.

A new form of the direct strength equation was developed to more directly control the influence of shape factor, stress redistribution, and residual strength. This novel form is a single curve from the plastic moment to strength at extreme slenderness utilizing two simple coefficients. Adjustment to these coefficients for stress redistribution and residual strength are made using rational relationships with neutral axis location and stable section depth. The results from these proposed equations were slightly better than the modified DSM equations for local buckling, and much-improved for distortional buckling.

The advantage of the proposed new form is its rational development providing greater control over factors influencing strength. The simple form of one equation has a seamless transition from buckling strength to inelastic reserve which reflects the natural curvature observed with tests. Further investigation is recommended for application of this form to compression members, beam-columns, and other limit states.

## References

- AISI (2016). *North American Specification for the Design of Cold-Formed Steel Structural Members*, American Iron and Steel Institute S100-16, Washington, DC.
- AS/NZS (2018). *Cold-Formed Steel Structures*, Australian/New Zealand Standard 4600:2018, Australia.
- Beale, R.G., Godley, M.H.R., Enjily, V. (2001). "A theoretical and experimental investigation into cold-formed channel sections in bending with the unstiffened flanges in compression." *Comput. Struct.*, 79, 2403-2411.
- Baur, S.W., LaBoube, R.A. (2001). "Behavior of Complex Hat Shape Cold-Formed Steel Members." *Proceedings of Structural Stability Research Council*, Ft. Lauderdale, FL. 403-417.
- Degtyarev, V.V. (2020) "Computational study of elastic buckling and post-buckling strength of steel decks in bending." *Proceedings of the Annual Stability Conference*, Atlanta, GA.
- Nuttayasakul, N., Easterling, W.S. (2003). "Cold-Formed Steel Flexural Members Undergoing Distortional and Euler Buckling." *Proceedings of Structural Stability Research Council*, Baltimore, MD. 339-355.
- Oey, O., Papangelis, J. (2020). "Nonlinear Analysis of Cold-Formed Channels Bent about the Minor Axis." *Proceedings of the Cold-Formed Steel Research Consortium Colloquium*. Baltimore, MD.
- Raebel, C.H., Gwozdz, D. (2017). "Experimental and Numerical Comparison of Flexural Capacity of Light Gage Cold Formed Steel Roof Deck." Milwaukee School of Engineering Report No. MSOE-CAECM-CVE-17-10.
- Schafer, B.W., Peköz, T. (1998). "Direct Strength Prediction of Cold-Formed Steel Members using Numerical Elastic Buckling Solutions." *Fourteenth International Specialty Conference on Cold-Formed Steel Structures*, Rolla, MO.
- Schafer, B.W. (2019). "Advances in the Direct Strength Method of cold-formed steel design." *Thin-Walled Structures*, 140, 533-541.
- SFIA (2018). *Technical Guide for Cold-Formed Steel Framing Products*. Steel Framing Industry Association, Falls Church, VA.
- Shifferaw, Y., Schafer, B.W. (2012) "Inelastic Bending Capacity of Cold-Formed Steel Members." *J. of Struct. Eng.*, 138 (4): 468-480.
- Yu, C., Schafer, B.W. (2003). "Local Buckling Tests on Cold-Formed Steel Beams." *J. of Struct. Eng.*, 129.
- Yu, C., Schafer, B.W. (2006). "Distortional Buckling Tests on Cold-Formed Steel Beams." *J. of Struct. Eng.*, 132.
- Yu, C., Schafer, B.W. (2007). "Simulation of Cold-Formed Steel Beams in Local and Distortional Buckling with Application to the Direct Strength Method." *J. Constr. Steel Res.*, 63 (5), 581-590.